UC Irvine
UC Irvine Previously Published Works

Title
Comparison of Methods for Calculating the Field Excited by a Dipole Near a 2-D Periodic Material

Permalink
https://escholarship.org/uc/item/5wj468x7

Journal
IEEE Transactions on Antennas and Propagation, 55(6)

ISSN
0018-926X

Authors
Capolino, Filippo
Jackson, David R
Wilton, Donald R
et al.

Publication Date
2007-06-01

DOI
10.1109/tap.2007.897348

Copyright Information
This work is made available under the terms of a Creative Commons Attribution License, availalbe at https://creativecommons.org/licenses/by/4.0/

Peer reviewed

eScholarship.org Powered by the California Digital Library
University of California

Comparison of Methods for Calculating the Field Excited by a Dipole Near a 2-D Periodic Material

Filippo Capolino, *Senior Member, IEEE*, David R. Jackson, *Fellow, IEEE*, Donald R. Wilton, *Fellow, IEEE*, and Leopold B. Felsen, *Life Fellow, IEEE*

Prof. L. B. Felsen particularly cared about field representations and Green's functions, and for this reason we dedicate this paper to him. He was involved in the 2-D counterpart [18] of the present 3-D study, and he followed the 3-D study with us until July 2005. Unfortunately he did not see the final version of this work.

***Abstract*—A comparison of methods for calculating the field from a single dipole source in the proximity of an infinite periodic artificial material (PAM) is given. A direct plane-wave expansion method (PWM) is compared with the "array scanning method" (ASM). The ASM is shown to be the most efficient method for sources that are close to the PAM, since it only requires integration in the wavenumber plane over the Brillouin zone rather than over the entire wavenumber plane. It is also shown how the ASM may be used to efficiently calculate the Fourier transform of the field at any aperture plane, which is useful for asymptotic analysis. The ASM is shown to be more efficient than the PWM or the reciprocity method for calculating the transform of the aperture field. A discussion of the nature of the singularities in the complex wavenumber plane is given, and numerical issues associated with the implementation of the ASM are discussed.**

***Index Terms*—Arrays, artificial materials, field representations, Green function, periodic structures.**

I. Introduction

PERIODIC artificial materials (PAM) have been the subject of great interest and have been increasingly applied to antennas and microwave devices [1]–[11]. As an example, electromagnetic band gap (EBG) materials are used to suppress surface-wave propagation [3]–[8]. In other applications, placing an antenna near/within a PAM has been shown to significantly affect the input impedance or to create directive beams [9]–[11]. Additionally, many leaky-wave antennas are in fact periodic in nature, and are excited by simple sources such as dipoles near the periodic structure [12], [13].

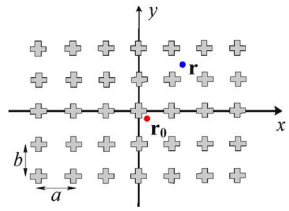

Fig. 1. Periodic structure made of a rectangular lattice of scatterers with dipole source at $\mathbf{r}_0$ and observation point at $\mathbf{r}$.

The present contribution is focused on the efficient calculation of the field due to a single (non-periodic) dipole source in the presence of an infinite three-dimensional PAM that is periodic in two dimensions and finite in the third. Some of the related numerical implementation issues are also discussed. The PAM under consideration is allowed to have an arbitrary metallization within the unit cell. Although the general case of a skewed lattice could be treated, the discussion is limited here to a rectangular lattice with periods a and b along the x and y axes, respectively. A typical periodic structure (with a metallic cross element) is shown in Fig. 1, which shows the dipole source location $\mathbf{r}_0 = (x_0, y_0, z_0)$ and the observation point $\mathbf{r} = (x, y, z)$. The methods discussed can easily be applied to layered structures having dielectric layers, but the discussion here will focus on structures in free space for simplicity.

It is first reviewed how the field produced by a dipole source in the presence of the infinite PAM may be calculated by a direct plane-wave expansion method (PWM). Although this method is well known and (as shown here) is not always an efficient method, it is useful as a benchmark for comparison.

The "array scanning method" (ASM) for calculating the field due to a single dipole source near an infinite PAM is then reviewed. This method has been introduced previously and used in the analysis of phased arrays [14]–[16]. The method has also been discussed recently in the context of analyzing the fields near one-dimensional (1-D) periodic artificial material structures [17]. The purpose here is to extend the investigation of the ASM to two dimensions, and to provide a comprehensive comparison of the method with other methods for analyzing two-dimensional artificial materials. The focus is on providing a general methodology that allows the ASM to be incorporated into general moment-method integral equation solvers. This paper represents the extension to the 3-D case (periodic in two directions and finite in the third direction) of the 2-D case (periodic in one direction, infinite in another direction, and finite in the

Manuscript received June 9, 2006; revised December 29, 2006. This work was supported in part by the EU-funded project METAMORPHOSE (FP6/NMP3-CT-2004-500252) and in part by the State of Texas Advanced Technology Program.

F. Capolino is with the Department of Information Engineering, University of Siena, Siena 53100, Italy (e-mail: capolino@dil.unisi.it).

D. R. Jackson and D. R. Wilton are with the Department of Electrical and Computer Engineering, University of Houston, TX 77204-4005 USA.

L. B. Felsen, *(deceased)*, was with the Department of Aerospace and Mechanical Engineering and the Department of Electrical and Computer Engineering, Boston University, Boston, MA 02215 USA, and also with Polytechnic University, Brooklyn, NY 11201 USA.

Color versions of one or more of the figures in this paper are available online at http://ieeexplore.ieee.org.

Digital Object Identifier 10.1109/TAP.2007.897348

0018-926X/$25.00 © 2007 IEEE

third direction) treated in [18] and the same formalism is used here.

In addition to providing a very efficient method for calculating the field of a dipole source, it is shown how the ASM may be used to efficiently calculate the Fourier transform of the field at any aperture plane of interest. This is useful for performing asymptotic analysis, since such analyses often start with the assumption that the relevant integrals that describe the field are in the form of an inverse transform integral. Having the field expressed in this form is also useful for complex path deformations to identify the types of wave phenomena that are present and to determine the launching amplitude of surface and leaky waves. It is shown that the ASM provides a more efficient calculation of the transform of the field than does the PWM or an alternative reciprocity-based method that is introduced.

In the ASM method the PAM is excited by an infinite periodic array of dipole sources with the same period as the PAM and phased with variable wavenumbers (k_x, k_y). An integration in (k_x, k_y) (i.e., scanning the phased dipole array) over the Brillouin region, $-\pi/a < k_x < \pi/a$ and $-\pi/b < k_y < \pi/b$, recovers the field produced by the single dipole source near the PAM.

An understanding of the nature of the k_x and k_y planes in the array scanning method is important for an asymptotic evaluation of the field along the interface of the PAM. It is shown that due to the periodic nature of the problem, there is an infinite set of branch point loci. Furthermore, there is also an infinite set of periodic pole loci that lead to surface and leaky waves. A discussion of these issues is given so that numerical aspects in the implementation of the ASM can be understood.

In Section II the PWM is reviewed. In Section III the array scanning method is discussed. In Section IV a comparison is given between the ASM and the direct PWM, and it is shown how the ASM field representation may be transformed into the PWM form. A comparison of computational efficiency between the PWM and the ASM is also given. The ASM representation is much more efficient when the source is close to the PAM, and this is discussed. In Section V it is shown how the solution from the ASM may be used to cast the solution in the form of a 2-D inverse Fourier transform integral, allowing for the efficient determination of the Fourier transform of the aperture field. In Section VI issues associated with the numerical implementation of the ASM are discussed, including singularities in the complex wavenumber plane and errors due to numerical integration. In Section VII numerical results are given that illustrate some of the features discussed in the previous section. Finally, in Section VIII conclusions are given.

II. Synthesis by Plane-Wave Superposition

Consider the problem illustrated in Fig. 1 where a PAM is excited by an impressed unit electric dipole current source at $\mathbf{r}_0 = x_0\hat{\mathbf{x}} + y_0\hat{\mathbf{y}} + z_0\hat{\mathbf{z}}$, oriented along the direction $\hat{\mathbf{J}}$ (which may be $\hat{\mathbf{x}}, \hat{\mathbf{y}}, \hat{\mathbf{z}}$ or any other direction), described by

$$\mathbf{J}^i(\mathbf{r}') = \hat{\mathbf{J}}\delta(\mathbf{r}' - \mathbf{r}_0) \tag{1}$$

where $\delta(\mathbf{r}' - \mathbf{r}_0) = \delta(x' - x_0)\delta(y' - y_0)\delta(z' - z_0)$. Here and in the following, boldface symbols are used to identify vector quantities and the caret "$\wedge$" identifies unit vectors. The PAM structure in Fig. 1 is periodic along x and y, with periods a and b, respectively. The structure may also be periodic along z, truncated after a finite number of layers, thereby constituting a slab of artificial material. In this case the term "supercell" is used to denote a unit cell in the x and y directions (which contains multiple cells spaced along z). For simplicity we consider here only metallic scatterers such as those shown in Fig. 1. In what follows, we represent a general observation point (which may be located in the (m, n)-th unit cell) as $\mathbf{r} + ma\hat{\mathbf{x}} + nb\hat{\mathbf{y}}$, where $\mathbf{r}$ is assumed to lie within the (0,0)-th unit cell. The field in free space at $\mathbf{r}$ radiated by the single dipole source at $\mathbf{r}_0$ is denoted by $\mathbf{E}_{\rm inc}(\mathbf{r}, \mathbf{r}_0)$ and it can be represented in terms of plane waves as

$$\mathbf{E}_{\rm inc}(\mathbf{r}, \mathbf{r}_0) = \frac{-j}{8\pi^2}\int_{-\infty}^{\infty}\int_{-\infty}^{\infty}\frac{1}{k_z}\underline{\mathbf{G}}(\mathbf{k}_t) \cdot \hat{\mathbf{J}}\, e^{-j[k_x(x-x_0)+k_y(y-y_0)-k_z|z-z_0|]}dk_x dk_y \tag{2}$$

$$\underline{\mathbf{G}}(\mathbf{k}_t) = \left[-j\omega\mu\underline{\mathbf{I}} \mp \frac{1}{j\omega\varepsilon}\mathbf{k}\mathbf{k}\right] \tag{3}$$

where $\mathbf{k} = k_x\hat{x} + k_y\hat{\mathbf{y}} + k_z\hat{\mathbf{z}}, k_z = \sqrt{k^2 - k_x^2 - k_y^2}$, and $k_t = k_x\hat{\mathbf{x}} + k_y\hat{\mathbf{y}}$ is the transverse part of $\mathbf{k}$. $\underline{\mathbf{I}}$ is the identity dyad. The "minus (plus)" sign is used when the observation point is above (below) the source point. Assuming the dipole source is above the periodic structure for simplicity, the incident field from the dipole source that illuminates the periodic structure is a continuum of plane waves of the form

$$\mathbf{E}_{\rm inc}^{\rm PW}(\mathbf{r}, \mathbf{r}_0, \mathbf{k}_t) = \hat{\mathbf{p}}(\mathbf{k}_t)W_{\rm inc}(\mathbf{k}_t, \mathbf{r}_0)e^{-j[k_x x + k_y y - k_z z]} \tag{4}$$

with

$$W_{\rm inc}(\mathbf{k}_t, \mathbf{r}_0) = \frac{-j}{8\pi^2}\frac{1}{k_z}\hat{\mathbf{p}}(\mathbf{k}_t)\cdot\underline{\mathbf{G}}(\mathbf{k}_t)\cdot\hat{\mathbf{J}}e^{j[k_x x_0 + k_y y_0 - k_z z_0]}. \tag{5}$$

Each incident plane wave in the spectrum is polarized in a direction $\hat{\mathbf{p}}(\mathbf{k}_t)$ where

$$\hat{\mathbf{p}}(\mathbf{k}_t) = \frac{\underline{\mathbf{G}}(\mathbf{k}_t)\cdot\hat{\mathbf{J}}}{\sqrt{(\underline{\mathbf{G}}(\mathbf{k}_t)\cdot\hat{\mathbf{J}})\cdot(\underline{\mathbf{G}}(\mathbf{k}_t)\cdot\hat{\mathbf{J}})^*}} \tag{6}$$

(the asterisk denotes complex conjugate). The scattered field due to a unit-amplitude incident plane wave $\bar{\mathbf{E}}_{\rm inc}^{\rm PW}(\mathbf{r}, \mathbf{k}_t) = \hat{\mathbf{p}}(\mathbf{k}_t)\mathbf{e}^{-j[k_x x + k_y y - k_z z]}$ with transverse wavevector $\mathbf{k}_t$ is denoted as $\bar{\mathbf{E}}_{\rm sca}^{\rm PW}(\mathbf{r}, \mathbf{k}_t)$. (A bar over a quantity is used here to signify that the quantity is either a unit-amplitude incident plane wave or is produced by such an incident wave.) Similarly, the total field due to a unit-amplitude incident plane wave is denoted as $\bar{\mathbf{E}}_{\rm tot}^{\rm PW}(\mathbf{r}, \mathbf{k}_t)$. From superposition, the scattered field produced by the dipole source in the PAM environment is evaluated by summing all the fields produced by each plane wave in (2). The scattered field produced by the single point source is thus

$$\mathbf{E}_{\rm sca}(\mathbf{r}, \mathbf{r}_0) = \int_{-\infty}^{\infty}\int_{-\infty}^{\infty}W_{\rm inc}(\mathbf{k}_t, \mathbf{r}_0)\bar{\mathbf{E}}_{\rm sca}^{\rm PW}(\mathbf{r}, \mathbf{k}_t)dk_x dk_y \tag{7}$$

and similarly for $\mathbf{E}_{\rm tot}$.

The electric field produced by a unit-amplitude incident plane wave $\bar{\mathbf{E}}_{\rm inc}^{\rm PW}(\mathbf{r}, \mathbf{k}_t)$ is found by first solving the electric field integral equation (EFIE) within the $(m, n) = (0, 0)$ supercell to

find the surface current $\bar{\mathbf{J}}_{S0}^{\mathrm{PW}}(\mathbf{r}', \mathbf{k}_t)$ on the elements within the supercell. The field scattered by the PAM is then given as

$$\bar{\mathbf{E}}_{\mathrm{sca}}^{\mathrm{PW}}(\mathbf{r}, \mathbf{k}_t) = \int_{S_0} \underline{\mathbf{G}}^{\infty}(\mathbf{r}, \mathbf{r}', \mathbf{k}_t) \cdot \bar{\mathbf{J}}_{S0}^{\mathrm{PW}}(\mathbf{r}', \mathbf{k}_t) dS'. \tag{8}$$

The free-space periodic Green's function is

$$\underline{\mathbf{G}}^{\infty}(\mathbf{r}, \mathbf{r}', \mathbf{k}_t) = \frac{1}{2jab} \sum_{p=-\infty}^{\infty} \sum_{q=-\infty}^{\infty} e^{-j(k_{xp}x + k_{yq}y)} \times \frac{1}{k_{zpq}} \underline{\mathbf{G}}(\mathbf{k}_{t,pq})\, e^{+j(k_{xp}x' + k_{yq}y' - k_{zpq}|z-z'|)} \tag{9}$$

where the dyad $\underline{\mathbf{G}}(\mathbf{k}_{t,pq})$ is given by (3) with $\mathbf{k}_t = \mathbf{k}_{t,pq}$ and the wavevector of each Floquet wave is $\mathbf{k}_{pq} = k_{xp}\hat{\mathbf{x}} + k_{yq}\hat{\mathbf{y}} + k_{zpq}\hat{\mathbf{z}}$, with transverse wavevector

$$\mathbf{k}_{t,pq} = k_{xp}\hat{\mathbf{x}} + k_{yq}\hat{\mathbf{y}} \tag{10}$$

where

$$k_{xp} = k_x + F_{xp}, \quad F_{xp} = \frac{2\pi p}{a} \tag{11}$$

$$k_{yq} = k_y + F_{yq}, \quad F_{yq} = \frac{2\pi q}{b}. \tag{12}$$

The longitudinal Floquet wavenumber along z is

$$k_{zpq} = \sqrt{k^2 - k_{xp}^2 - k_{yq}^2} \tag{13}$$

where k is the free-space wavenumber. As will be clear later, it is convenient to exhibit the singularity $1/k_{zpq}$ explicitly in (9).

Branch points are defined from $k_{xp}^2 + k_{yq}^2 = k^2$, corresponding to $k_{zpq} = 0$. Therefore, if k_y is fixed, there is a doubly infinite set of branch points in the k_x plane at

$$k_{xb,pq}^{\pm}(k_y) = \pm\sqrt{k^2 - k_{yq}^2} - F_{xp}. \tag{14}$$

If the k_x integral is performed first in the double integration of (7), as indicated by the integration order, then the path of integration lies in the complex k_x plane for each value of k_y. The path stays on the top Riemann sheet of all the branch points, and the wavenumber k_{zpq} is chosen as either purely real and positive or purely imaginary with a negative imaginary part (assuming a lossless medium). Geometrically, the location of the branch points for a given value of k_y is determined by the intersection of a horizontal line (constant k_y) with the circles shown in Fig. 2.

The field radiated by the scattering structure when illuminated by a unit-amplitude incident plane wave can be expressed as a Floquet expansion, so that

$$\bar{\mathbf{E}}_{\mathrm{sca}}^{\mathrm{PW}}(\mathbf{r}, \mathbf{k}_t) = \sum_{p=-\infty}^{\infty} \sum_{q=-\infty}^{\infty} e^{-j(k_{xp}x + k_{yq}y)} \bar{\mathbf{e}}_{\mathrm{sca},pq}^{\mathrm{PW}}(z, \mathbf{k}_t). \tag{15}$$

Insertion of (9) into (8) yields

$$\bar{\mathbf{e}}_{\mathrm{sca},pq}^{\mathrm{PW}}(z, \mathbf{k}_t) = \frac{-j}{2ab} \frac{1}{k_{zpq}} \underline{\mathbf{G}}(\mathbf{k}_{t,pq}) \cdot \int_{S_0} \bar{\mathbf{J}}_{S0}^{\mathrm{PW}}(\mathbf{r}', \mathbf{k}_t)\, e^{+j[k_{xp}x' + k_{yq}y' - |z-z'|k_{zpq}]} dS'. \tag{16}$$

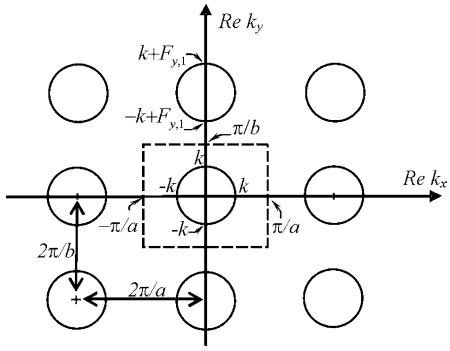

Fig. 2. Periodic branch-point loci in the plane $\mathrm{Re}k_x, \mathrm{Re}k_y$. The area contained within the dashed line represents the Brillouin zone that is used in the ASM.

Note that (15) represents the Floquet wave expansion of the scattered field. The term $\bar{\mathbf{e}}_{\mathrm{sca},pq}^{\mathrm{PW}}$ physically represents the amplitude of the (p,q)th Floquet mode that is scattered by the PAM due to a unit-amplitude incident plane wave. The scattered field produced by the dipole source is then represented as

$$\mathbf{E}_{\mathrm{sca}}(\mathbf{r}, \mathbf{r}_0) = \int_{-\infty}^{\infty} \int_{-\infty}^{\infty} W_{\mathrm{inc}}(\mathbf{k}_t, \mathbf{r}_0) \times \sum_{p=-\infty}^{\infty} \sum_{q=-\infty}^{\infty} e^{-j(k_{xp}x + k_{yq}y)} \bar{\mathbf{e}}_{\mathrm{sca},pq}^{\mathrm{PW}}(z, \mathbf{k}_t) dk_x dk_y. \tag{17}$$

A significant numerical effort may be required to evaluate the scattered field from this equation since it involves a 2-D infinite integral and a 2-D infinite sum. This is particularly true when the source point lies vertically close (in the z direction) to the PAM, since the weight function $W_{\mathrm{inc}}(\mathbf{k}_t, \mathbf{r}_0)$ then contributes minimally to the convergence of the integrations for large values of k_t. In fact, as the source dipole approaches the PAM, the weight function $W_{\mathrm{inc}}(\mathbf{k}_t, \mathbf{r}_0)$ defined in (5) does not tend to zero as $k_t \to \infty$. However, in a periodic moment-method solution, the integral of the incident electric field over the basis functions on the unit supercell would be required for the computation of the right-hand elements, and this integration (which results in the Fourier transform of the basis functions) would result in a converging integral expression.

For source points that are well removed from the PAM, the integration converges rapidly, and is limited to essentially the visible space region ($|\mathbf{k}_t| \leqslant k_0$). The ASM for calculating the scattered field, which remains efficient even for sources close to the PAM, is discussed in the next section.

III. The Array Scanning Method (ASM)

The single dipole source $\mathbf{J}^i(\mathbf{r}')$ in (1) oriented along the direction $\hat{\mathbf{J}}$ can be realized by using the "array scanning method," [14]–[16], i.e., by synthesizing the single dipole source from an infinite phased array of identical point sources located at $\mathbf{r}_{mn} = \mathbf{r}_0 + ma\hat{\mathbf{x}} + nb\hat{\mathbf{y}}$, as shown in Fig. 3. Mathematically, the phased array of dipole sources is represented as

$$\mathbf{J}^{i,\infty}(\mathbf{r}', \mathbf{k}_t) = \hat{\mathbf{J}} \sum_{\mathrm{m}=-\infty}^{\infty} \sum_{n=-\infty}^{\infty} \delta(\mathbf{r}' - \mathbf{r}_{mn}) e^{-j(k_x ma + k_y nb)}. \tag{18}$$

The wavenumbers k_x and k_y are the phasing gradients along the x and y directions, respectively. According to the ASM [15], the

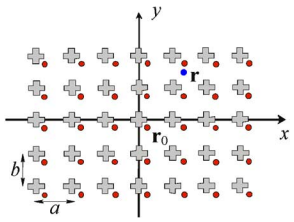

Fig. 3. Periodic structure excited by an infinite set of phased dipole sources at locations $\mathbf{r}_{mn} = \mathbf{r}_0 + ma\hat{\mathbf{x}} + nb\hat{\mathbf{y}}$. The original dipole source is located at $\mathbf{r}_0$.

current of the single dipole can be obtained by integrating (18) over the Brillouin zone shown in Fig. 2, so that

$$\mathbf{J}^i(\mathbf{r}') = \frac{ab}{(2\pi)^2}\int_{-\pi/a}^{\pi/a}\int_{-\pi/b}^{\pi/b}\mathbf{J}^{i,\infty}(\mathbf{r}',\mathbf{k}_t)dk_x dk_y. \quad (19)$$

Physically, this represents the fact that when the phased array currents $\mathbf{J}^{i,\infty}(\mathbf{r}',\mathbf{k}_t)$ are integrated in $\mathbf{k}_t$ over the Brillouin zone, all of the currents located at $\mathbf{r}_{mn}$ in the phased array integrate to zero except the one located at $(m,n) = (0,0)$. The incident field generated by $\mathbf{J}^{i,\infty}(\mathbf{r}',\mathbf{k}_t)$ is represented as $\mathbf{E}^{\infty}_{\rm inc}(\mathbf{r},\mathbf{r}_0,\mathbf{k}_t) = \underline{\mathbf{G}}^{\infty}(\mathbf{r},\mathbf{r}_0,\mathbf{k}_t)\cdot\hat{\mathbf{J}}$, where the periodic dyadic Green's function $\underline{\mathbf{G}}^{\infty}(\mathbf{r},\mathbf{r}_0,\mathbf{k}_t)$ is given in (9). The incident field is thus rewritten as

$$\mathbf{E}^{\infty}_{\rm inc}(\mathbf{r},\mathbf{r}_0,\mathbf{k}_t) = \sum_{p=-\infty}^{\infty}\sum_{q=-\infty}^{\infty} e^{-j(k_{xp}x+k_{yq}y)} \times\mathbf{e}^{\infty}_{{\rm inc},pq}(z,\mathbf{r}_0,k_t) \quad (20)$$

with

$$\mathbf{e}^{\infty}_{{\rm inc},pq}(z,\mathbf{r}_0,\mathbf{k}_t) = \frac{1}{2jab}\frac{1}{k_{zpq}}\underline{\mathbf{G}}(\mathbf{k}_{t,pq}) \cdot\hat{\mathbf{J}}e^{+j(k_{xp}x_0+k_{yq}y_0-k_{zpq}|z-z_0|)}. \quad (21)$$

The incident field exhibits an infinite set of (pq)-indexed branch loci in the (k_x,k_y) plane defined by the equation for $k_{xp}^2+k_{yq}^2 = k^2$ that, for fixed k_y, define the doubly infinite set of branch points in (14). The scattered field can then be represented as a sum of scattered Floquet waves of the form

$$\mathbf{E}^{\infty}_{\rm sca}(\mathbf{r},\mathbf{r}_0,\mathbf{k}_t) = \sum_{p=-\infty}^{\infty}\sum_{q=-\infty}^{\infty} e^{-j(k_{xp}x+k_{yq}y)} \times\mathbf{e}^{\infty}_{{\rm sca},pq}(z,\mathbf{r}_0,\mathbf{k}_t) \quad (22)$$

where

$$\mathbf{e}^{\infty}_{{\rm sca},pq}(z,\mathbf{r}_0,\mathbf{k}_{t,pq}) = \frac{1}{2jab}\frac{1}{k_{zpq}}\underline{\mathbf{G}}(\mathbf{k}_{t,pq}) \cdot\int_{S_0}\mathbf{J}^{\infty}_{S0}(\mathbf{r}',\mathbf{r}_0,\mathbf{k}_t)e^{+j[k_{xp}x'+k_{yq}y'-|z-z'|k_{zpq}]}dS' \quad (23)$$

and $\mathbf{J}^{\infty}_{S0}(\mathbf{r}',\mathbf{r}_0,\mathbf{k}_t)$ is the current on the scatterers in the (0,0) supercell, when excited by the infinite phased array of dipoles. This current is obtained from a numerical solution of the EFIE on the (0,0) supercell using a periodic moment-method code. The current $\mathbf{J}^{\infty}_{S0}(\mathbf{r}',\mathbf{r}_0,\mathbf{k}_t)$ is a periodic function of the spectral variable $\mathbf{k}_t$, with periods $2\pi/a$ and $2\pi/b$ in k_x and k_y, respectively, since the phased array of dipole sources is periodic in k_x, and k_y.

According to the ASM, the current on the PAM is obtained from the infinite phased-array current by a spectral integration over the Brillouin zone, so that

$$\mathbf{J}_S(\mathbf{r},\mathbf{r}_0) = \frac{ab}{(2\pi)^2}\int_{-\pi/a}^{\pi/a}\int_{-\pi/b}^{\pi/b}\mathbf{J}^{\infty}_S(\mathbf{r},\mathbf{r}_0,\mathbf{k}_t)dk_x dk_y. \quad (24)$$

The scattered and total fields produced by the single dipole source are also obtained by a spectral integration over the Brillouin zone, so that

$$\mathbf{E}_{\rm sca}(\mathbf{r},\mathbf{r}_0) = \frac{ab}{(2\pi)^2}\int_{-\pi/a}^{\pi/a}\int_{-\pi/b}^{\pi/b}\mathbf{E}^{\infty}_{\rm sca}(\mathbf{r},\mathbf{r}_0,\mathbf{k}_t)dk_x dk_y \quad (25)$$

and

$$\mathbf{E}_{\rm tot}(\mathbf{r},\mathbf{r}_0) = \frac{ab}{(2\pi)^2}\int_{-\pi/a}^{\pi/a}\int_{-\pi/b}^{\pi/b}\mathbf{E}^{\infty}_{\rm tot}(\mathbf{r},\mathbf{r}_0,\mathbf{k}_t)dk_x dk_y. \quad (26)$$

The field $\mathbf{E}^{\infty}_{\rm tot}(\mathbf{r},\mathbf{r}_0,\mathbf{k}_t) = \mathbf{E}^{\infty}_{\rm inc}(\mathbf{r},\mathbf{r}_0,\mathbf{k}_t) + \mathbf{E}^{\infty}_{\rm sca}(\mathbf{r},\mathbf{r}_0,\mathbf{k}_t)$ may be conveniently represented as a sum of Floquet waves, as

$$\mathbf{E}^{\infty}_{\rm tot}(\mathbf{r},\mathbf{r}_0,\mathbf{k}_t) = \sum_{p=-\infty}^{\infty}\sum_{q=-\infty}^{\infty} e^{-j(k_{xp}x+k_{yq}y)} \times\mathbf{e}^{\infty}_{{\rm tot},pq}(z,\mathbf{r}_0,\mathbf{k}_t) \quad (27)$$

where

$$\mathbf{e}^{\infty}_{{\rm tot},pq}(z,\mathbf{r}_0,\mathbf{k}_t) = \mathbf{e}^{\infty}_{{\rm inc},pq}(z,\mathbf{r}_0,\mathbf{k}_t) + \mathbf{e}^{\infty}_{{\rm sca},pq}(z,\mathbf{r}_0,\mathbf{k}_t). \quad (28)$$

The integrands $\mathbf{E}^{\infty}_{\rm sca}(\mathbf{r},\mathbf{r}_0,\mathbf{k}_t)$ and $\mathbf{E}^{\infty}_{\rm tot}(\mathbf{r},\mathbf{r}_0,\mathbf{k}_t)$ are both periodic functions of k_x, and k_y with periods $2\pi/a$ and $2\pi/b$, respectively. The singularities of the integrands of (25) and (26) are discussed in Section VI, and they are important to determine the proper numerical treatment of the integrals (see [17] for a similar problem with 1-D periodicity).

One important property of the ASM is that it only involves the calculation of a field from a *periodic source* (for either the incident or scattered field), and for this type of calculation highly efficient acceleration schemes may be used, such as the Ewald method [19]. In fact the Ewald method may be used to calculate both the incident and scattered fields, instead of using (21) and (23). The Ewald method represents the periodic free-space Green's function as a sum of two double series, each of each has Gaussian convergence. Typically, each double series in the Ewald method converges with summation limits from -2 to 2. In all of the numerical calculations performed later, the Ewald method was used.

In the expressions for the surface current $\mathbf{J}_S(\mathbf{r},\mathbf{r}_0)$ and the electric fields $\mathbf{E}_{\rm sca}(\mathbf{r},\mathbf{r}_0)$ and $\mathbf{E}_{\rm tot}(\mathbf{r},\mathbf{r}_0)$ we can assume for convenience and without loss of generality that the point $\mathbf{r}$ is located within the (0,0) unit cell and that the observation point

is now described by $\mathbf{r}+ma\hat{\mathbf{x}}+nb\hat{\mathbf{y}}$. In this case expressions (24), (25), and (26) can be rewritten as

$$\mathbf{F}(\mathbf{r}+ma\hat{\mathbf{x}}+nb\hat{\mathbf{y}},\mathbf{r}_0) = \frac{ab}{(2\pi)^2}\int_{-\pi/a}^{\pi/a}\int_{-\pi/b}^{\pi/b}\mathbf{F}^{\infty}(\mathbf{r},\mathbf{r}_0,\mathbf{k}_t) \times e^{-j(k_x ma+k_y nb)}dk_x dk_y \quad (29)$$

where $\mathbf{F}^{\infty}(\mathbf{r},\mathbf{r}_0,\mathbf{k}_t)$ denotes either $\mathbf{J}_{S0}^{\infty}(\mathbf{r},\mathbf{r}_0,k_t)$, $\mathbf{E}_{\rm sca}^{\infty}(\mathbf{r},\mathbf{r}_0,\mathbf{k}_t)$, or $\mathbf{E}_{\rm tot}^{\infty}(\mathbf{r},\mathbf{r}_0,\mathbf{k}_t)$.

IV. Relation Between the ASM and the Plane-Wave Superposition Method

A. Equivalence of Methods

By noticing that the incident field $\mathbf{E}_{\rm inc}^{\infty}(\mathbf{r},\mathbf{r}_0,\mathbf{k}_t)$ in (20) produced by the infinite phased array of dipoles $\mathbf{J}^{i,\infty}(\mathbf{r}',\mathbf{k}_t)$ in the ASM can be viewed as a weighted superposition of plane waves, the relation between the scattered field $\mathbf{E}_{\rm sca}^{\infty}(\mathbf{r},\mathbf{r}_0,\mathbf{k}_t)$ produced by $\mathbf{J}^{i,\infty}(\mathbf{r}',\mathbf{k}_t)$ and the field $\bar{\mathbf{E}}_{\rm sca}^{\rm PW}(\mathbf{r},\mathbf{k}_t)$ produced by a unit-amplitude incident plane wave may be written as

$$\mathbf{E}_{\rm sca}^{\infty}(\mathbf{r},\mathbf{r}_0,\mathbf{k}_t) = \sum_{p=-\infty}^{\infty}\sum_{q=-\infty}^{\infty}\frac{1}{2jab}\frac{c_{pq}}{k_{zpq}}\bar{\mathbf{E}}_{\rm sca}^{\rm PW}(\mathbf{r},\mathbf{k}_{t,pq}) \quad (30)$$

with

$$c_{pq} = \hat{\mathbf{p}}(\mathbf{k}_{t,pq})\cdot\underline{\mathbf{G}}(\mathbf{k}_{t,pq})\cdot\hat{\mathbf{J}}e^{+j(k_{xp}x_0+k_{yq}y_0-k_{zpq}z_0)}. \quad (31)$$

Similarly, the current $\mathbf{J}_{S0}^{\infty}(\mathbf{r}',\mathbf{r}_0,\mathbf{k}_{t,pq})$ on the (0,0) supercell induced by $\mathbf{J}^{i,\infty}(\mathbf{r}',\mathbf{k}_t)$ is

$$\mathbf{J}_{S0}^{\infty}(\mathbf{r}',\mathbf{r}_0,\mathbf{k}_t) = \sum_{p=-\infty}^{\infty}\sum_{q=-\infty}^{\infty}\frac{1}{2jab}\frac{c_{pq}}{k_{zpq}}\bar{\mathbf{J}}_{S0}^{\rm PW}(\mathbf{r}',\mathbf{k}_{t,pq}). \quad (32)$$

The scattered field calculated by the ASM may then be cast into the form

$$\mathbf{E}_{\rm sca}(\mathbf{r},\mathbf{r}_0) = \frac{ab}{(2\pi)^2}\int_{-\pi/b}^{\pi/b}\int_{-\pi/a}^{\pi/a}\frac{1}{2jab} \times\sum_{p=-\infty}^{\infty}\sum_{q=-\infty}^{\infty}\frac{c_{pq}}{k_{zpq}}\bar{\mathbf{E}}_{\rm sca}^{\rm PW}(\mathbf{r},\mathbf{k}_{\mathbf{t},pq})dk_x dk_y. \quad (33)$$

Mathematically, (7) is seen to be equivalent to (33) by using the fact that

$$\int_{-\infty}^{\infty}\int_{-\infty}^{\infty}W_{\rm inc}(\mathbf{k}_t,\mathbf{r}_0)\bar{\mathbf{E}}_{\rm sca}^{\rm PW}(\mathbf{r},\mathbf{k}_t)dk_x dk_y = \sum_{p=-\infty}^{\infty}\sum_{q=-\infty}^{\infty}\int_{-\pi/a}^{\pi/a}\int_{-\pi/b}^{\pi/b}W_{\rm inc}(\mathbf{k}_{t,pq},\mathbf{r}_0) \times\bar{\mathbf{E}}_{\rm sca}^{\rm PW}(\mathbf{r},\mathbf{k}_{t,pq})dk_x dk_y \quad (34)$$

in order to transform the wavenumber integrations from the entire real axis into one over the Brillouin zone.

The integrand $\mathbf{E}_{\rm sca}^{\infty}(\mathbf{r},\mathbf{r}_0,\mathbf{k}_t)$ in (25) can in principle be calculated using (30). However, doing so requires the solution of an infinite number of plane-wave scattering problems. A much more efficient method is to directly calculate $\mathbf{E}_{\rm sca}^{\infty}(\mathbf{r},\mathbf{r}_0,\mathbf{k}_t)$ by numerically solving the problem of an infinite set of phased dipole sources above the PAM. This numerical solution requires a periodic moment-method analysis that is essentially no more numerically intensive than that for a single plane wave scattering problem.

The advantage of the ASM is that (25) requires a spectral integration that is carried out *only* over the Brillouin zone in contrast to (17), which requires an integration over the entire (k_x,k_y) plane. (However, as mentioned previously, for source points that are well removed from the PAM, the integration in (17) will converge very rapidly.)

TABLE I
The Ratio R, Giving the Computational Effort of the PWM Relative to That of the ASM, for Various Vertical Separations of the Source From the Periodic Structure

$\lvert z_0-z'\rvert/\lambda$	R ($\Delta/\lambda=0.025$)	R ($\Delta/\lambda=0.25$)
100	0.79	0.79
10	0.80	0.81
5	0.83	0.86
2	1.0	1.1
1	1.8	1.7
0.1	1.6E+02	39
0.01	7.9E+03	1.3E+03
0	2.2 E+09	2.2E+05

B. Numerical Comparison of Methods

To clarify the comparison of computational efficiency between the ASM and the PWM, both methods may be compared in terms of how many periodic moment-method solutions they require in order to determine the current on the PAM due to the original source dipole (the determination of the current on the structure is often the most time-consuming step). The details of this comparison are provided in the Appendix. A ratio R is defined as the number of periodic moment-method solutions required in the PWM relative to the number required in the ASM. The ratio R depends dramatically on the vertical separation $k_0|z_0-z'|$, where z' is the z coordinate of the PAM (assuming for the sake of simplicity that it is planar here). From the analysis in the Appendix, it is seen that for very large vertical separations, R is roughly on the order of

$$R\approx\pi\left(\frac{a}{\lambda_0}\right)\left(\frac{b}{\lambda_0}\right),\quad k_0|z_0-z'|\to\infty. \quad (35)$$

However, as $k_0|z_0-z'|$ decreases the ratio R increases, with the rate determined by the size of the testing basis/testing functions used in the moment-method solution for the PAM.

Table I gives the value of R calculated from the rough order-of-estimate formula (55) for a typical case having $a/\lambda_0 = b/\lambda_0 = 0.5$. In this comparison the half-length Δ of each testing function is assumed to be one of two values: either 0.025λ (representing a typical sub-domain basis function) or 0.25λ (representing a typical full-domain basis function). It is seen that for large separations the PWM has a slight advantage, while for small separations the ASM has a large advantage. According to this (rather crude) estimate, the ASM becomes more efficient for a vertical spacing that is less than about two wavelengths. For large vertical separations the size of the basis functions is inconsequential, but for larger separations it is obvious that using smaller basis functions results in a much slower convergence in the PWM.

V. Fourier Transform of Aperture Field

The calculation of the transform of the field on the aperture plane of the periodic structure (or any other plane located at a fixed value of z) is important for performing asymptotic analysis, and for identifying the launching amplitude of surface and leaky waves. Therefore, this calculation is considered here. Three methods for calculating the transform are discussed and compared.

A. Plane-Wave Expansion Method

Starting from (17), the scattered field may be put in terms of an inverse Fourier transform integral by "collecting the spectrum." That is, all of the plane waves that have a wavevector $\mathbf{k}_t$ are summed together. Mathematically, this is equivalent to using the change of variables $k_x = k'_x - F_{xp}$ and $k_y = k'_y - F_{yq}$ for each term of the sum in (17), followed by the substitution $p \to -p$ and $q \to -q$, and results in the expression

$$\mathbf{E}_{\rm sca}(\mathbf{r},\mathbf{r}_0) = \int_{-\infty}^{\infty}\int_{-\infty}^{\infty} e^{-j(k_x x+k_y y)} \sum_{p=-\infty}^{\infty}\sum_{q=-\infty}^{\infty} W_{\rm inc}(\mathbf{k}_{t,pq},\mathbf{r}_0) \times \bar{\mathbf{e}}^{\rm PW}_{{\rm sca},(-p)(-q)}(z,\mathbf{k}_{\rm tpq})dk_x dk_y. \quad (36)$$

The scattered field thus has the inverse Fourier transform representation

$$\mathbf{E}_{\rm sca}(\mathbf{r},\mathbf{r}_0) = \frac{1}{4\pi^2}\int_{-\infty}^{\infty}\int_{-\infty}^{\infty} e^{-j(k_x x+k_y y)} \tilde{\mathbf{E}}_{\rm sca}(z,\mathbf{r}_0,\mathbf{k}_t)dk_x dk_y \quad (37)$$

where

$$\tilde{\mathbf{E}}_{\rm sca}(z,\mathbf{r}_0,\mathbf{k}_t) = 4\pi^2 \sum_{p=-\infty}^{\infty}\sum_{q=-\infty}^{\infty} W_{\rm inc}(\mathbf{k}_{t,pq},\mathbf{r}_0) \times \bar{\mathbf{e}}^{\rm PW}_{{\rm sca},(-p)(-q)}(z,\mathbf{k}_{t,pq}). \quad (38)$$

Considering the definition of the $W_{\rm inc}$ function in (5), expression (38) explicitly shows that the integrand $\tilde{\mathbf{E}}^{\rm PW}_{\rm sca}$ has an infinite set of branch point loci, located at $k_{xp}^2 + k_{yq}^2 = k^2$ [see the discussion after (13)].

Although (38) is a valid expression for the Fourier transform of the field at any z value, it may be numerically intensive to compute, since it requires the numerical solution of an infinite number of scattering problems involving an incident plane wave (i.e., an infinite number of incidence angles corresponding to wavevectors $\mathbf{k}_{t,pq}$.) However, as mentioned previously, the weight function $W_{\rm inc}(\mathbf{k}_t,\mathbf{r}_0)$ decays rapidly with increasing p and q when the source point is well separated from the PAM, so that expression (38) eventually becomes quite efficient for large separations. In the next section an efficient method for obtaining the Fourier transform using the ASM is presented, which remains efficient even for small separations between the PAM and the source point.

B. Array Scanning Method

It is possible to "unfold" the integration path from the Brillouin zone shown in Fig. 2 to the entire (k_x, k_y) plane. Doing so allows for a convenient identification and calculation of the Fourier transform of the field at any fixed height z. The path unfolding is done by first inserting (22) into (25), and then using the property that

$$\mathbf{e}^{\infty}_{{\rm sca},pq}(z,\mathbf{r}_0,\mathbf{k}_t) = \mathbf{e}^{\infty}_{{\rm sca},00}(z,\mathbf{r}_0,\mathbf{k}_{t,pq}). \quad (39)$$

The shift of variables $k_x + F_{xp} \to k_x$ and $k_y + F_{yq} \to k_y$ is applied for every (p,q) term of the sum, leading to

$$\mathbf{E}_{\rm sca}(\mathbf{r},\mathbf{r}_0) = \frac{ab}{(2\pi)^2}\int_{-\infty}^{\infty}\int_{-\infty}^{\infty} e^{-j(k_x x+k_y y)} \times \mathbf{e}^{\infty}_{{\rm sca},00}(z,\mathbf{r}_0,\mathbf{k}_t)dk_x dk_y \quad (40)$$

where $\mathbf{E}^{\infty}_{{\rm sca},00}(z,\mathbf{r}_0,\mathbf{k}_t)$ is calculated using (23) and the supercell current $\mathbf{J}^{\infty}_{S0}(\mathbf{r}',\mathbf{r}_0,\mathbf{k}_t)$. By comparing (40) with (37) the Fourier transform of the scattered field is identified as

$$\tilde{\mathbf{E}}_{\rm sca}(z,\mathbf{r}_0,\mathbf{k}_t) = ab\,\mathbf{e}^{\infty}_{{\rm sca},00}(z,\mathbf{r}_0,\mathbf{k}_t). \quad (41)$$

Equation (41) indicates that the Fourier transform of the aperture field is (to within the simple constant ab) the same as the amplitude of the (0,0) Floquet wave that is radiated by the PAM when it is excited by the phased array of dipole sources. It is straightforward to extract the amplitude of this fundamental Floquet wave from the periodic moment-method solution with the phased array of dipole sources.

In the case of field evaluation at a point z larger than all the z-points of the scatterer (i.e., when $z \geqslant z'$ for all $z' \in S_0$) a simple explicit expression for the amplitude of the scattered fundamental Floquet wave (and hence the transform of the scattered field) can be derived (an analogous result applies when z is smaller than all the z-points of the scatterer.) Using (40) and (23) leads to

$$\tilde{\mathbf{E}}_{\rm sca}(z,\mathbf{r}_0,\mathbf{k}_t) = \frac{1}{2j}\frac{1}{k_z}\underline{\mathbf{G}}(\mathbf{k}_t)\cdot\tilde{\mathbf{J}}^{\infty}_{S0}(\mathbf{r}_0,\mathbf{k}_t)e^{-jk_z z} \quad (42)$$

where

$$\tilde{\mathbf{J}}^{\infty}_{S0}(\mathbf{r}_0,\mathbf{k}_t) = \int_{S_0}\mathbf{J}^{\infty}_{S0}(\mathbf{r}',\mathbf{r}_0,\mathbf{k}_t)e^{j(k_x x'+k_y y'+k_z z')}dS' \quad (43)$$

is the *three-dimensional* Fourier transform of the current $\mathbf{J}^{\infty}_{S0}(\mathbf{r}',\mathbf{r}_0,\mathbf{k}_t)$ on the unit cell.

C. Reciprocity Method

The reciprocity method may be used to provide an alternative calculation of the Fourier transform of the total field at any fixed z plane. Assume that the transform of the l component of the electric field ($l = x, y, z$ or any other direction) is to be calculated at $z = z_F$ for transform wavevectors $k_t = (k_x, k_y)$. An infinite "testing current" sheet of the form

$$\mathbf{J}^{\rm test}(x,y,\mathbf{k}_t) = \hat{\mathbf{l}}\,e^{+j(k_x x+k_y y)} \quad (44)$$

is placed at z_F. Dot multiplying the scattered electric field from the PAM due to the dipole source with the testing current and integrating over the plane at $z = z_F$ yields the Fourier transform of the l component of the electric field at z. By reciprocity [20], this is equivalent to calculating the electric field radiated by the testing current sheet (in the presence of the PAM) and sampling the $\hat{\mathbf{J}}$ component of the field at the source dipole location $\mathbf{r}_0$. The incident field radiated by the current sheet in (44) is

$$\mathbf{E}_{\text{test}}(\mathbf{r}) = \frac{1}{2jk_z}(\underline{\mathbf{G}}(-\mathbf{k}_t)\cdot\hat{\mathbf{l}})e^{+j[k_x x + k_y y - k_z|z-z_F|]}. \quad (45)$$

This field is a plane-wave field that impinges on the PAM, and the total resulting field is then sampled in the $\hat{\mathbf{J}}$ direction at $\mathbf{r}_0$ to yield $\tilde{\mathbf{E}}_{\text{sca}}(z, \mathbf{r}_0, \mathbf{k}_t)$.

The reciprocity calculation requires a plane-wave excitation of the PAM for each wavevector $\mathbf{k}_t$. In comparison, the ASM formula (41) requires the excitation of the PAM by a phased array of dipole sources. Both problems require the same level of computational effort. However, in the ASM, a calculation of the phased-array dipole problem with wavenumbers ranging over the Brillouin zone is sufficient to reconstruct the Fourier transform for all wavenumbers in the entire (k_x, k_y) plane. This is because of property (39).

Of course, in the numerical calculation of the Floquet waves (the left-hand side of (39)), enough Floquet terms must be calculated to ensure that the wavevector $\mathbf{k_t}_{,pq} = \mathbf{k}_t + \hat{\mathbf{x}}F_{xp} + \hat{\mathbf{y}}F_{yq}$ extends over the desired range for which the transform is being computed. In view of (39) and (41), the Fourier transform is known over the entire (k_x, k_y) plane once the phased-array scattering problem has been solved for all wavenumbers within the Brillouin zone. Hence, the ASM is much more efficient numerically than the reciprocity method in calculating the complete Fourier transform for all wavenumbers (k_x, k_y). If the transform is only desired for a limited range of wavenumbers, the reciprocity method is of comparable efficiency.

VI. Numerical Issues

A. Singularities

In performing the k_x integration in (25) or (26), branch-point singularities may be encountered on the real axis of the k_x plane. There is a doubly infinite set of branch points at $k_{xb,pq}^{\pm}(k_y)$ in the k_x plane, given by (14) and shown in Fig. 4. The branch points are periodic along the real axis, with period $2\pi/a$. In the central Brillouin zone, defined as $-\pi/a < \text{Re}k_x < \pi/a$, there are an infinite number of branch points along the imaginary axis. There may be a pair of branch points on the real axis, depending on the value of the integration variable k_y. When $kb < \pi$ and $2\pi m/b + k < k_y < 2\pi(m+1)/b - k$ there will not be any branch points on the real k_x axis. (This means that in Fig. 2 the branch-point circles do not intersect vertically, and the horizontal k_y line passes through one of the vertical gaps between the circles.) Otherwise, there will be at least one pair of branch points on the real axis.

In many practical cases the frequency is low enough so that $ka < \pi$ and $kb < \pi$, and there will then be at most one pair of branch points on the real k_x axis within the integration region $-\pi/a < k_x < \pi/a$, and all the others will lie on the imaginary

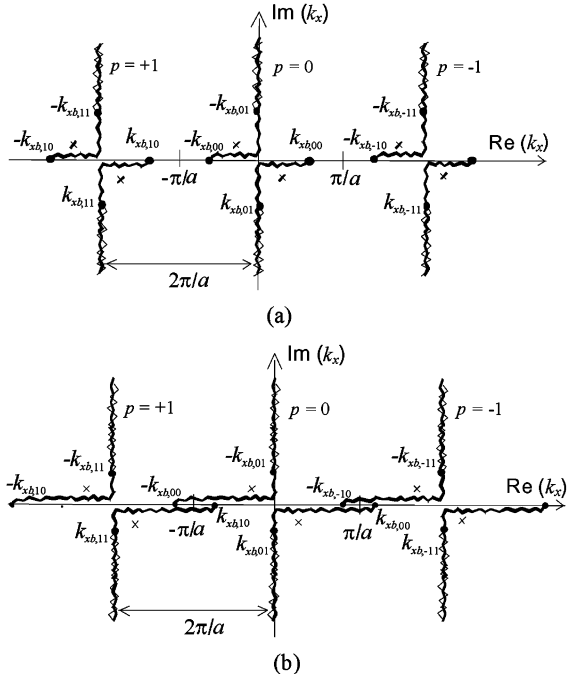

Fig. 4. Spectral k_x plane, for a fixed k_y value. The poles (the $\mathbf{x}$ points below the branch cut) and branch points are periodic in the k_x plane, with period $2\pi/a$. (a) case with $ka < \pi$, or equivalently $a/\lambda < 1/2$, (b) case with $ka > \pi$.

k_x axis. This is the case shown in Fig. 4(a). The integration in the complex k_x plane in the region $-\pi/a < k_x < \pi/a$ can be deformed off of the real axis to avoid the branch points on the real axis.

When $ka > \pi$, branch cuts corresponding to adjacent values of p in (14) may overlap on the real k_x axis as shown in Fig. 4(b). This will happen when $k_y^2 < k^2 - (\pi/a)^2$. In this situation it is not possible to deform the path to avoid the branch points in the integration region when staying on the top Riemann sheet. Hence, this case requires careful integration along the real axis, especially in the region where the branch cuts overlap.

It is also interesting to note that the integrand of (25) is more singular at the branch points than is the integrand of (26). This is because of the physical fact that the scattered field from the source decays with distance more slowly along the PAM than does the total field. The decay of the scattered field is $1/r$, which matches that of the incident field (the two must cancel on the conducting surfaces of the PAM). However the total field has a more rapid decay of $1/r^2$ far away from the source, which is typical of the behavior observed in any interface problem, including, e.g., a source over a dielectric layer. Hence, especially when evaluating the scattered field, care must be taken to integrate accurately near the branch points, or to deform around them if possible (for the case of Fig. 4(a). The behavior of the fields is verified numerically in the next section.

There may also appear surface-wave poles on the real axis if the PAM allows for the guidance of such waves. In the case of Fig. 4(a), where $k_x a < \pi$, deforming the path off the real axis will allow for the avoidance of such poles. In the case of Fig. 4(b), where $k_x a > \pi$, it is not possible to deform the path entirely off the real axis (staying on the top Riemann sheet). However, in this case all guiding modes must be leaky modes

[21], because at least one Floquet wave is a radiating fast wave for all k_x values within the Brillouin zone. Hence, the leaky-wave poles will lie off the real k_x axis.

Leaky modes may also exist in addition to surface waves, in the case of Fig. 4(a). (Leaky-mode poles are denoted with crosses in the figure.) The leaky modes may cause numerical difficulty if they are close to the real axis, but this is an unusual situation unless the PAM has been designed to form a leaky-wave antenna type of structure.

The above discussion of singularities in the complex k_x plane is common to both the ASM and the PWM. In the PWM the integration is over the entire $k_x - k_y$ plane, and hence the integration in k_x is over the entire k_x axis instead of only the region $(-\pi/a, \pi/a)$ in Fig. 4.

B. Numerical Integration Error

If the integrals (25) and (26) are approximated by sampling uniformly the integrand in the Brillouin zone, a physical interpretation of the numerical error can be given. Besides providing a simple physical interpretation of the error, the use of the "midpoint rectangle rule" of integration is chosen because it is especially accurate for periodic functions, and in particular for those cases where the integrand is smooth [22]. Sampling the integrand at points

$$k_x = \xi_p = -\frac{\pi}{a} + \frac{2\pi}{aP}(p - 1/2) \tag{46}$$

$$k_y = \eta_q = -\frac{\pi}{b} + \frac{2\pi}{bQ}(q - 1/2) \tag{47}$$

with $p = 1, \ldots P$ and $q = 1, \ldots Q$, i.e., at the center of each of the (P, Q) intervals (i.e., the midpoint rectangle rule), leads to an interesting physical interpretation of the error. In particular, the error in approximating the field at a location $\mathbf{r}$ due to a dipole source at $\mathbf{r}_0$ is equivalent to summing the field produced by an infinite number of dipole source "images" located at $\mathbf{r}_0 + mPa\hat{\mathbf{x}} + nQb\hat{\mathbf{y}}$ for $m, n = \pm 1, \pm 2, \ldots$ (the proof is omitted here). The integration approximation is thus satisfactory when the nearest images (those with $m = \pm 1, n = \pm 1,$) are sufficiently far away, i.e., P and Q are large enough to result in a large spatial field decay from the nearest images. One interesting ramification of this is the fact that if the medium is lossy, the error eventually decreases *exponentially* with an increasing number of integration points. This surprising result is consistent with the discussion in [22], which shows how the error in the simple midpoint rectangle rule often has exponentially small errors when integrating smooth periodic functions. The loss makes the integrand smooth over the integration region, since branch points are now located off the real axis. For lossless cases, adaptive integration schemes are possible as a way to improve the numerical integration, with a coarser sampling away from the singularities in the complex k_x plane and a finer sampling close to the singularities.

VII. Results

Results are obtained using a uniform sampling (rectangle integration rule) to perform the numerical integrations, as discussed in Section VI-B. The array of scatterers is made of resonant strip-dipoles with length $L = 0.5\lambda$, where λ is the free-space wavelength, and width $W = 0.07\lambda$, oriented along x. The metal dipole in the (0,0) unit cell is divided into 10 rectangular subdomains of length $d = 0.05\lambda$ and 9 rectangular rooftop basis functions are used. The array is a square lattice with element spacings $a = b = 0.7\lambda$. The source is an elementary x-directed electric dipole with a unit amplitude ($Il = 1$ Am) located at $\mathbf{r}_0 = -0.2\lambda\hat{\mathbf{x}} - 0.2\lambda\hat{\mathbf{y}} + 0.0\lambda\hat{\mathbf{z}}$ (the origin is at the center of the (0,0) metal strip dipole). The current I (in amps) is calculated on the metal dipoles at a distance d from the left end of each dipole. Results are presented for the current on dipole $(0, n)$ centered at $(x, y) = (0, nb)$, where n is varied in the results below.

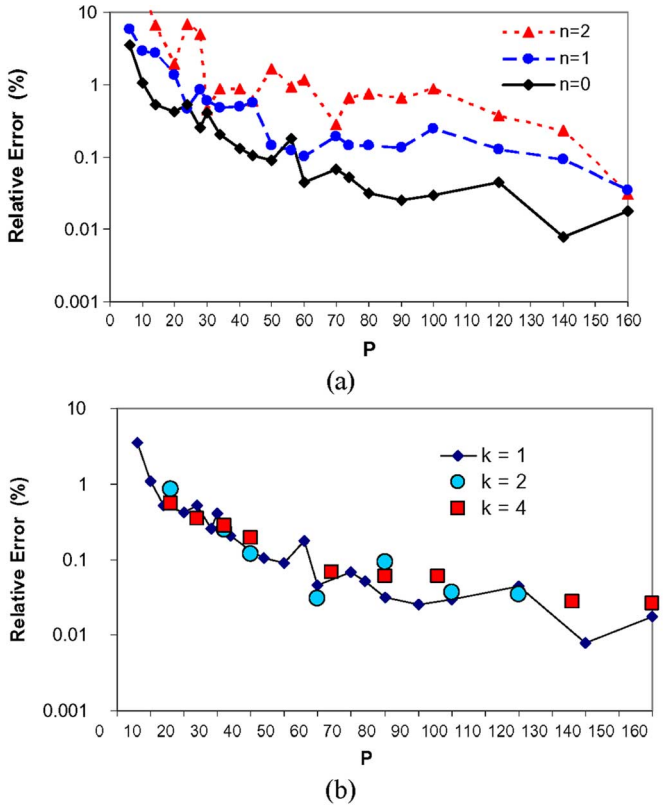

Fig. 5. The percent error in the current on the metal dipoles calculated by using the ASM versus the number of sample points along k_x or k_y, with the same number $P = Q$ of equidistant sampling points in (46) and (47). (a) Error shown for three different (0,n) metal dipoles when using the midpoint rectangle rule of integration. (b) Error shown for the (0,0) metal dipole for three different orders of Gaussian quadrature ($k = 1$ is equivalent to using the midpoint rectangle rule).

In Fig. 5 we show the percent error in the current defined as $|I^{\mathrm{ASM}} - I^{\mathrm{ref}}|/|I^{\mathrm{ref}}| \times 100$, where I^{ref} represents the current on the metal dipoles obtained using many integration points ($P = Q = 600$), but keeping the number of basis functions fixed at nine. The error thus calculated is therefore a measure of the error in the numerical integration over the Brillouin zone. In Fig. 5(a) the three curves represent the percent error at three different supercell locations, corresponding to $n = 0, 1, 2$, along the y-direction. The current I^{ASM} is evaluated via the ASM described in Section III, using (29) to evaluate the surface current on the metal dipoles. The ASM is performed by integrating over the real k_x and k_y axes, with the same number $P = Q$ of equidistant sampling points in (46) and (47), corresponding to a total number of P^2 sampling points in the $k_x - k_y$ plane. Fig. 5 shows the above mentioned error versus P. Because the

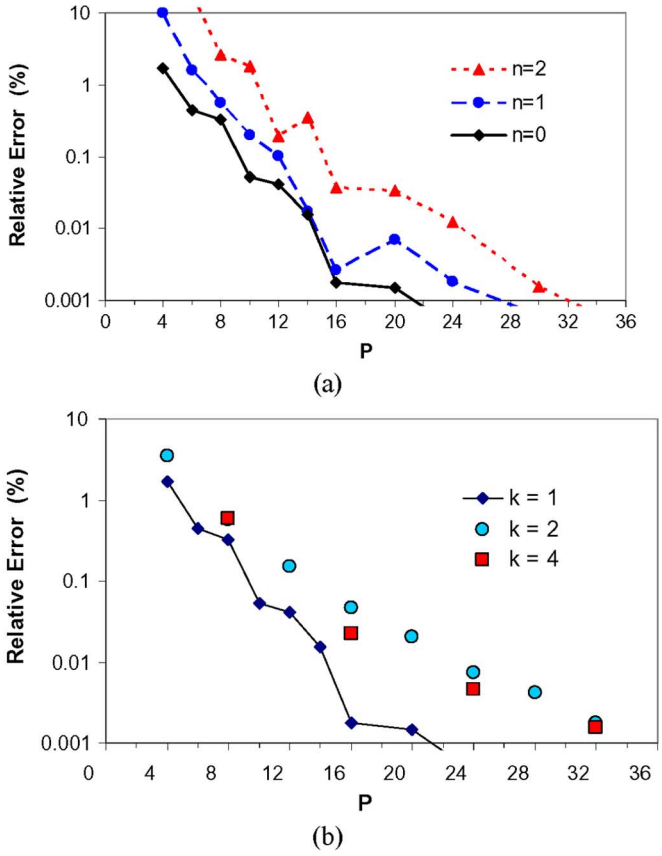

Fig. 6. The same result as for Fig. 5, but for a lossy air medium that has a loss tangent of 0.1.

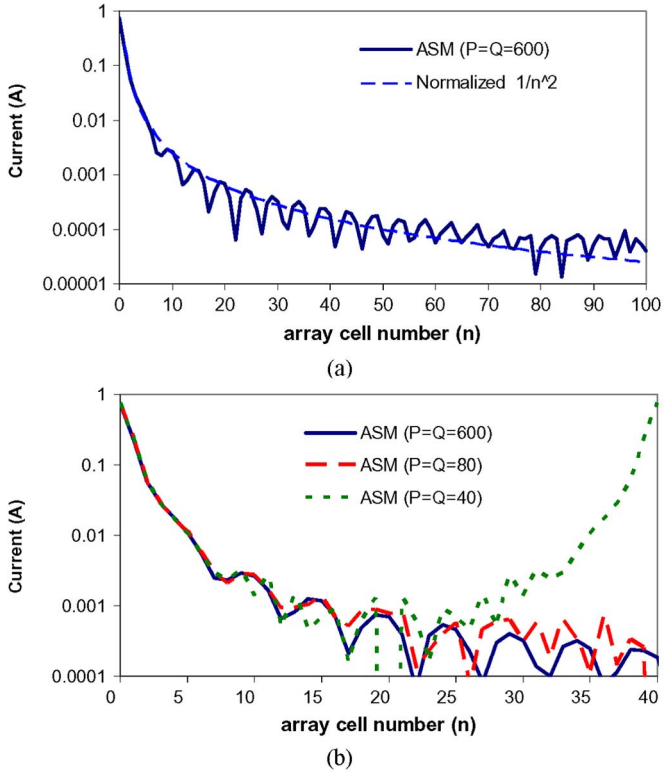

Fig. 7. The current on the metal dipoles calculated by using the ASM versus the number of cells away from the (0,0) cell in the y direction. (a) A result is shown using a large number of integration points. Also shown is a normalized $1/n^2$ curve for comparison. (b) Results are shown for various numbers of integration points.

periodic structure is in free space, the periodic Green's function employed in the moment-method solution for the currents has been evaluated using the Ewald method [19], which is much more efficient than a direct evaluation of (9). The Ewald method has been used to calculate the incident field from the phased array of sources in the ASM, and also to calculate the field from the periodic currents on the metal dipoles in the ASM, which is used to generate the matrix elements in the moment-method system of equations.

Fig. 5(a) shows that the relative error is larger for those metal dipoles that are further away from the source because the field produced by the source is weaker there and the effect of the nearest "images" at $\mathbf{r}_0 + mPa\hat{\mathbf{x}} + nQb\hat{\mathbf{y}}$, for $m = \pm 1, n = \pm 1$, is thus relatively stronger (see the discussion in Section VI-B). In Fig. 5(b) the percent error is plotted for $n = 0$ (the metal dipole in the (0,0) cell), using Gaussian quadrature with three different orders ($k = 1, 2$, and 4). In this comparison P equals the order k times the number of subintervals used in the integration. Using order $k = 1$ (one sample point per subinterval of integration) is equivalent to the midpoint rectangle rule of integration, and hence the $k = 1$ curve is identical to the $n = 0$ curve in Fig. 5(a). The results show that the error is about the same when using the midpoint rule as with Gaussian quadrature (see the discussion in Section VI-B for an explanation of why the midpoint rectangle rule is expected to work well).

Fig. 6 shows the same result as in Fig. 5, but for a lossy case where the air medium now has a loss tangent of 0.1. Comparing Figs. 6(a) and 5(a), it is seen that the loss significantly increases the convergence rate of the numerical integration. This is because the lossless case of Fig. 5(a) had branch points on the real axis within the range of integration. Adding loss moves the branch points off the real axis, resulting in a smoother integrand. Equivalently, the addition of loss renders the field produced by the "images," the reason for the error when using the midpoint rectangle integration rule, weaker. The midpoint rectangle rule now outperforms Gaussian quadrature, as Fig. 6(b) shows. The error also decreases exponentially with the number of integration points, as expected from the discussion in Section VI-B.

In Fig. 7(a) the current is plotted over the first 100 metal dipoles along the y direction (n varies from 0 to 100). The field decay follows the expected behavior $1/r^2$ as seen by the addition of the normalized $1/n^2$ curve. The curve has noticeable oscillations, which are not due to numerical error ($P = Q = 600$ is sufficient to guarantee accurate results). Evidently, this is due to interference between the main space wave and a weaker mode (perhaps a leaky mode) propagating along the PAM interface.

In Fig. 7(b) the field is plotted again along the y direction using an accurate solution ($P = Q = 600$) that is compared with that obtained using $P = Q = 80$ and $P = Q = 40$. Using fewer integration points causes loss of accuracy away from the source. For $P = Q = 40$ points the effects of the nearest "image" source in cell $n = 40$ is clearly visible. The null at $n = 20$ is caused by the cancellation of the field produced by the source and this image.

VIII. Conclusion

A comparison of methods for calculating the field due to a single dipole source in the presence of an infinite periodic artificial material (PAM) has been provided. A direct plane-wave expansion method (PWM) has been compared with the "array scanning method" (ASM), and the latter was shown to be much more numerically efficient when the source is located close to the PAM, since it only requires an integration over the Brillouin zone rather than over the entire wavenumber plane.

For some applications, such as asymptotic analysis and calculation of surface-wave and leaky-wave modal amplitudes, it is also important to be able to calculate the Fourier transform of the field at some aperture plane, so that the field is in the form of an inverse transform integral. Three methods were compared for the calculation of the transform: (1) the PWM, (2) the ASM, and (3) a reciprocity-based method. Of these, the array scanning method is the most efficient. The PWM requires the solution of an infinite number of scattering problems (i.e., different incident waves impinging on the PAM) in order to determine the transform for a given set of wavenumbers (k_x, k_y). The ASM and the reciprocity method require only a single scattering problem. However, the array scanning method allows for the complete transform to be constructed from the scattering solution for incident wavenumbers that are within the Brillouin zone.

The nature of the complex plane in the wavenumber integration of the ASM was discussed in some detail, including the location of the branch points and well as surface-wave and leaky-wave poles. An understanding of the singularities in the complex plane is important for numerical implementation. A physical discussion of the error involved in approximating the integrations with discrete samples was also given to help understand the numerical error that arises in the method.

Appendix

In this Appendix a rough estimate is given for the ratio R, defined as the number of numerical periodic moment-method calculations required to obtain the current on the PAM in the PWM relative to that in the ASM.

ASM: The number of required solutions is

$$N_{\rm ASM} = \left(\frac{2\pi}{a}\right)\left(\frac{2\pi}{b}\right) D_x^{\rm ASM} D_y^{\rm ASM} \tag{48}$$

where $D_x^{\rm ASM}$ is the numerical integration sampling density in k_x and $D_y^{\rm ASM}$ is the sampling density in k_y.

PWM: For simplicity, assume that E_x is being calculated from an x-directed dipole source. In a periodic moment-method solution, the right-hand side terms in the moment-method system of equations represent the integration of the incident field over the testing functions (assumed here to be the same as the basis functions). For simplicity a representative basis function is assumed here to be x directed, with the current in the x direction described by a function $w(x)$. The integration in x over the basis function yields the Fourier transform $\tilde{w}(k_x)$. To establish a convergence condition, we take $k_y = 0$ for simplicity and focus only on k_x, and then require that k_x be large enough so that the integration of the incident E_x field from the source dipole in (2) over the testing function on the PAM is negligible compared to that for $k_x = 0$ (the result has decreased by a factor of $\exp(-A)$, where A is a somewhat arbitrary number, typically around 2π). This yields the result

$$\frac{1}{\omega\varepsilon}\frac{k_x k_x}{\sqrt{k_x^2 - k_0^2}} e^{-\sqrt{k_x^2 - k_0^2}\,\Delta_z} \tilde{w}(k_x) = e^{-A}\left(\omega\mu\frac{1}{k_0}\right)\tilde{w}(0) \tag{49}$$

where $\Delta_z = |z_0 - z'|$ with z' being the coordinate of the PAM (assumed to be planar here), and the left-hand side arises from the leading contribution in (2) for large k_x. Writing this in a normalized form, we have

$$\left(\frac{\tilde{w}(k_x)}{\tilde{w}(0)}\right)\frac{\bar{k}_x^2}{\sqrt{\bar{k}_x^2 - 1}} e^{-\sqrt{\bar{k}_x^2 - 1}(k_0\Delta_z)} = e^{-A} \tag{50}$$

where $\bar{k}_x = k_x/k_0$. To be explicit, we assume here that

$$w(x) = \cos\left(\frac{\pi x}{2\Delta}\right), \quad |x| < \Delta \tag{51}$$

with

$$\tilde{w}(k_x) = \left(\frac{\pi\Delta}{2}\right)\frac{\cos(k_x\Delta)}{(\pi/2)^2 - (k_x\Delta)^2}. \tag{52}$$

Taking the maximum of the cosine function, we have from (50) that

$$\left(\frac{1}{1 - \left(\frac{2}{\pi}\bar{k}_x(k_0\Delta)\right)^2}\right)\frac{\bar{k}_x^2}{\sqrt{\bar{k}_x^2 - 1}} e^{-\sqrt{\bar{k}_x^2 - 1}(k_0\Delta_z)} = e^{-A}. \tag{53}$$

The solution to the above transcendental equation is denoted as $\bar{k}_x = \bar{k}_x^{\rm LIM}$. Note that as $k_0\Delta_z \to \infty, \bar{k}_x^{\rm LIM} \to 1$ (the incident spectrum is confined to the visible-space circle). On the other hand, as $k_0\Delta_z \to 0$, the limit is determined by the rate of convergence of $\tilde{w}(k_x)$.

If it is assumed that the numerical integration is performed over a circular region in the $k_x - k_y$ wavenumber plane, then the number of integration points required in the PWM is

$$N_{\rm PWM} = \pi k_0^2 \left(\bar{k}_x^{\rm LIM}\right)^2 D_x^{\rm PWM} D_y^{\rm PWM}. \tag{54}$$

If we assume that the sampling densities are the same in both methods, so that $D_x^{\rm ASM} = D_x^{\rm PWM}$ and $D_y^{\rm ASM} = D_y^{\rm PWM}$, we have that

$$R = \frac{N_{\rm PWE}}{N_{\rm ASM}} = \pi\left(\frac{k_0 a}{2\pi}\right)\left(\frac{k_0 b}{2\pi}\right)\left(\bar{k}_x^{\rm LIM}\right)^2 = \pi\left(\frac{a}{\lambda_0}\right)\left(\frac{b}{\lambda_0}\right)\left(\bar{k}_x^{\rm LIM}\right)^2. \tag{55}$$

References

[1] P.-S. Kildal, "Artificially soft and hard surfaces in electromagnetics," *IEEE Trans. Antennas Propag.*, vol. 38, no. 10, pp. 1537–1544, Oct. 1990.

[2] P. A. Belov, S. A. Tretyakov, and A. J. Viitanen, "Dispersion and reflection properties of artificial media formed by regular lattices of ideally conducting wires," *J. Electromagn. Waves Appl.*, vol. 16, no. 8, pp. 1153–1170, 2002.
[3] Z. Ying and P.-S. Kildal, "Improvements of dipole, helix, spiral, microstrip patch and aperture antennas with ground planes by using corrugated soft surfaces," *Proc. Inst. Elect. Eng. Microwaves, Antennas and Propagation*, vol. 143, no. 3, pp. 244–248, Jun. 1996.
[4] D. Sievenpiper, L. Zhang, R. Broas, N. G. Alexopoulos, and E. Yablonovitch, "High-impedance electromagnetic surfaces with a forbidden frequency band," *IEEE Trans. Microw. Theory Tech.*, vol. 47, no. 11, pp. 2059–2074, Nov. 1999.
[5] R. Gonzalo, P. de Maagt, and M. Sorolla, "Enhanced patch-antenna performance by suppressing surface waves using photonic-bandgap substrates," *IEEE Trans. Antennas Propag.*, vol. 47, no. 11, pp. 2131–2138, Nov. 1999.
[6] H. Y. D. Yang, R. Kim, and D. R. Jackson, "Design considerations for modeless integrated circuit substrates using planar periodic patches," *IEEE Trans. Microwave Theory Tech.*, vol. 48, no. 12, pp. 2233–2239, Dec. 2000.
[7] E. I. Smirnova, C. Chen, M. A. Shapiro, J. R. Sirigiri, and R. J. Temkin, "Simulation of photonic band gaps in metal rod lattices for microwave applications," *J. Appl. Phys.*, vol. 91, no. 3, pp. 960–968, Feb. 1, 2002.
[8] R. B. Hwang and S. T. Peng, "Surface-wave suppression of resonance-type periodic structures," *IEEE Trans. Antennas Propag.*, vol. 51, no. 6, pp. 1221–1229, Jun. 2003.
[9] H. Y. Yang and D. R. Jackson, "Theory of line-source radiation from a metal-strip grating dielectric-slab structure," *IEEE Trans. Antennas Propag.*, vol. 48, pp. 556–564, Apr. 2000.
[10] S. Enoch, G. Tayeb, P. Sabouroux, N. Guérin, and P. Vincent, "A metamaterial for directive emission," *Phy. Rev. Lett.*, vol. 89, no. 21, pp. 213902-1–213902-4, Nov. 2002.
[11] G. Lovat, P. Burghignoli, F. Capolino, D. R. Jackson, and D. R. Wilton, "Analysis of directive radiation from a line source in a metamaterial slab with low permittivity," *IEEE Trans. Antennas Propag.*, vol. 54, pp. 1017–1030, Mar. 2006.
[12] T. Zhao, D. R. Jackson, J. T. Williams, H. Y. Yang, and A. A. Oliner, "2-D periodic leaky-wave antennas—Part I: Metal patch design," *IEEE Trans. Antennas Propag.*, vol. 53, pp. 3505–3514, Nov. 2005.
[13] T. Zhao, D. R. Jackson, and J. T. Williams, "2-D periodic leaky-wave antennas—Part II: Slot design," *IEEE Trans. Antennas Propag.*, vol. 53, pp. 3515–3524, Nov. 2005.
[14] R. Sigelmann and A. Ishimaru, "Radiation from periodic structures excited by an aperiodic source," *IEEE Trans. Antennas Propag.*, vol. 13, no. 3, pp. 354–364, May 1965.
[15] C. P. Wu and V. Galindo, "Asymptotic behavior of the coupling coefficients for an infinite array of thin-walled rectangular waveguides," *IEEE Trans. Antennas Propag.*, vol. 14, pp. 248–249, Mar. 1966.
[16] B. A. Munk and G. A. Burrell, "Plane-wave expansion for arrays of arbitrarily oriented piecewise linear elements and its application in determining the impedance of a single linear antenna in a lossy half-space," *IEEE Trans. Antennas Propag.*, vol. 27, pp. 331–343, May 1979.
[17] F. Capolino, D. R. Jackson, and D. R. Wilton, "Fundamental properties of the field at the interface between air and a periodic artificial material excited by a line source," *IEEE Trans. Antennas Propag. Special Issue on Artificial Magnetic Conductors, Soft/Hard Surfaces, and Other Complex Surfaces*, vol. 53, pp. 91–99, Jan. 2005.
[18] F. Capolino, D. R. Jackson, D. R. Wilton, and L. B. Felsen, "Representation of the field excited by a line source near a 2-D periodic artificial material," in *Fields, Networks, Computational Methods, and Systems in Modern Electrodynamics*, P. Russer and M. Mongiardo, Eds. Berlin: Springer-Verlag, 2004, pp. 13–24, ISBN 3540-23929-4.
[19] S. Oroskar, D. R. Jackson, and D. R. Wilton, "Efficient computation of the 2-D periodic Green's function using the Ewald method," *J. Comput. Phys.*, vol. 219, pp. 899–911, 2006, doi:10.1016/j.jcp.2006.06.050.
[20] R. Harrington, *Time-Harmonic Electromagnetic Fields*. Piscataway, NJ: IEEE Press, 2001.
[21] A. A. Oliner, "Leaky-wave antennas," in *Antenna Engineering Handbook*, R. C. Johnson, Ed. New York: McGraw-Hill, 1993, ch. 10.
[22] J. A. C. Weideman, "Numerical integration of periodic functions: A few examples," *Amer. Mathematical Monthly*, vol. 109, no. 11, pp. 21–36, Jan. 2002.

Filippo Capolino (S'94–M'97–SM'04) was born in Florence, Italy, in 1967. He received the Laurea degree (*cum laude*) in electronic engineering and the Ph.D. degree from the University of Florence, Florence, Italy, in 1993 and 1997, respectively.

He is presently employed as an Assistant Professor at the Department of Information Engineering of the University of Siena, Italy. From 2000 to 2001 and in 2006, he was a Research Assistant Visiting Professor with the Department of Electrical and Computer Engineering, University of Houston, Houston, TX, where he is also an Adjunct Assistant Professor. From November to December 2003, he was an Invited Assistant Professor at the Institut Fresnel, Marseille, France. His research interests include theoretical and applied electromagnetics focused on high-frequency, short-pulse radiation, array antennas, periodic structures, numerical modelling, and metamaterials. He is the coordinator of the Siena Unit for the European Network of Excellence "Metamorphose" on Metamaterials.

Dr. Capolino was awarded with an MMET'94 Student Paper Competition Award in 1994, the Raj Mittra Travel Grant for Young Scientists in 1996, and for Senior Scientists in 2006, the "Barzilai" prize for the best paper at the National Italian Congress of Electromagnetism (XI RiNEm) in 1996, and a Young Scientist Award for participating at the URSI Int. Symp. Electromagn. Theory in 1998. He received the R. W. P. King Prize Paper Award from the IEEE Antennas and Propagation Society for the Best Paper of the Year 2000, by an author under 36. He is an Associate Editor for the IEEE TRANSACTIONS ON ANTENNAS AND PROPAGATION.

David R. Jackson (S'83–M'84–SM'95–F'99) was born in St. Louis, MO, on March 28, 1957. He received the B.S.E.E. and M.S.E.E. degrees from the University of Missouri, Columbia, in 1979 and 1981, respectively, and the Ph.D. degree in electrical engineering from the University of California, Los Angeles, in 1985.

From 1985 to 1991, he was an Assistant Professor in the Department of Electrical and Computer Engineering, University of Houston, Houston, TX, where from 1991 to 1998, he was an Associate Professor and since 1998 he has been a Professor. His present research interests include microstrip antennas and circuits, leaky-wave antennas, leakage and radiation effects in microwave integrated circuits, periodic structures, and EMC. He has served as an Associate Editor of *Radio Science* and the *International Journal of RF and Microwave Computer-Aided Engineering*.

Dr. Jackson is presently serving as the Chair of the Transnational Committee of the IEEE AP-S Society, and as the Chair for URSI, U.S. Commission B. He is a member of the Editorial Board of the IEEE TRANSACTIONS ON MICROWAVE THEORY AND TECHNIQUES. Previously, he has been the Chapter Activities Coordinator for the IEEE AP-S Society, a Distinguished Lecturer for the AP-S Society, an Associate Editor for the IEEE TRANSACTIONS ON ANTENNAS AND PROPAGATION, and a member of the AdCom for the AP-S Society.

Donald R. Wilton (S'63–M'65–SM'80–F'87) was born in Lawton, OK, on October 25, 1942. He received the B.S., M.S., and Ph.D. degrees from the University of Illinois at Urbana-Champaign, in 1964, 1966, and 1970, respectively.

From 1965 to 1968 he was with Hughes Aircraft Co., Fullerton, CA, engaged in the analysis and design of phased array antennas. From 1970 to 1983, he was with the Department of Electrical Engineering, University of Mississippi, and since 1983 he has been Professor of electrical engineering at the University of Houston. From 1978 to 1979 he was a Visiting Professor at Syracuse University. During 2004 to 2005 he was a Visiting Professor at the Polytechnic of Turin, Italy, the Sandia National Laboratories, and the University of Washington. His primary research interest is in computational electromagnetics, and he has published, lectured, and consulted extensively in this area.

Dr. Wilton is a member of Commission B of the International Union of Radio Science (URSI), in which he has held various offices including Chair of U. S. Commission B. He received the IEEE Third Millennium Medal. He has served the IEEE Antennas and Propagation Society as an Associate Editor of the IEEE TRANSACTIONS ON ANTENNAS AND PROPAGATION, as a Distinguished National Lecturer, and as a member of AdCom.

Leopold B. Felsen *deceased*, (S'47–M'54–SM'55–F'62–LF'90) was born in Munich, Germany, on May 7, 1924. He received the B.E.E., M.E.E, and D.E.E. degrees from the Polytechnic Institute of Brooklyn, Brooklyn, NY, in 1948, 1950, and 1952, respectively.

He emigrated to the United States in 1939 and served in the U.S. Army from 1943 to 1946. After 1952, he remained with the Polytechnic (now Polytechnic University), becoming University Professor in 1978. From 1974 to 1978, he was Dean of Engineering. In 1994, he resigned from the full-time Polytechnic faculty and was granted the status of University Professor Emeritus. He was Professor of aerospace and mechanical engineering and Professor of electrical and computer engineering at Boston University, Boston, MA (part-time). He was the author or coauthor of more than 350 papers and of several books, including *Radiation and Scattering of Waves* (Piscataway, NJ: IEEE Press, 1994). He was an Associate Editor of several professional journals and was an Editor of the *Wave Phenomena Series* (New York: Springer-Verlag). His research interests encompassed wave propagation and diffraction in complex environments and in various disciplines, high-frequency asymptotic and short-pulse techniques, and phase-space methods with an emphasis on wave-oriented data processing and imaging.

Dr. Felsen was a Member of Sigma Xi and a Fellow of the Optical Society of America and the Acoustical Society of America. He has held named Visiting Professorships and Fellowships at universities in the United States and abroad, including the Guggenheim in 1973 and the Humboldt Foundation Senior Scientist Award in 1981. In 1974 he was an IEEE Antennas and Propagation Society (APS) Distinguished Lecturer. His "Poet's Corner" appeared sporadically in the IEEE/APS Magazine. He received the IEEE/APS Best Paper Award for 1969 and was best paper coauthor for 1974 and 1981. He was a contributing author to papers selected for the R. W. P. King Award for 1984, 1986, and 2000. He received the Balthasar van der Pol Gold Medal from the International Union of Radio Science (URSI) in 1975, an Honorary Doctorate from the Technical University of Denmark in 1979, the IEEE Heinrich Hertz Gold Medal for 1991, the APS Distinguished Achievement Award for 1998, the IEEE Third Millennium Medal in 2000, an Honorary Laurea degree from the University of Sannio in Benevento, Italy in 2003, the IEEE Electromagnetics Award for 2003, an honorary doctorate from the Technical University of Munich, Germany in 2004, an Honorary Doctorate from Dogus University in Istanbul, Turkey, three Distinguished Faculty Alumnus Awards from Polytechnic University, and an IEEE Centennial Medal in 1984. In 1977, he was elected to the National Academy of Engineering. He served on the APS Administrative Committee from 1963 to 1966 and was Vice Chairman and Chairman for both the US (1966–1973) and the International (1978–1984) URSI Commission B.